Refractometric monitoring of dissolution and fluid flow with distributed feedback dye laser sensor

Vannahme, Christoph; Sørensen, Kristian Tølbøl; Gade, Carsten; Dufva, Martin; Kristensen, Anders

Published in:
Optics Express

Link to article, DOI:
10.1364/OE.23.006562

Publication date:
2015

Document Version
Publisher's PDF, also known as Version of record

Refractometric monitoring of dissolution and fluid flow with distributed feedback dye laser sensor

Christoph Vannahme,* Kristian Tølbøl Sørensen, Carsten Gade, Martin Dufva, and Anders Kristensen

Department of Micro- and Nanotechnology, Technical University of Denmark, DTU Nanotech, Ørsteds Plads, Building 345E, DK-2800 Kgs. Lyngby, Denmark
christoph.vannahme@nanotech.dtu.dk

Abstract: Monitoring the dissolution of solid material in liquids and monitoring of fluid flow is of significant interest for applications in chemistry, food production, medicine, and especially in the fields of microfluidics and lab on a chip. Here, real-time refractometric monitoring of dissolution and fast fluid flow with DFB dye laser sensors with an optical imaging spectroscopy setup is presented. The dye laser sensors provide both low detection limits and high spatial resolution. It is demonstrated how the materials NaCl, sucrose, and bovine serum albumin show characteristic dissolution patterns. The unique feature of the presented method is a high frame rate of up to 20 Hz, which is proven to enable the monitoring of fast flow of a sucrose solution jet into pure water.

OCIS codes: (140.0140) Lasers and laser optics; (110.0110) Imaging systems; (280.3420) Laser sensors; (140.3490) Lasers, distributed-feedback.

References and links

1. W. Min, "Label-free optical imaging of nonfluorescent molecules by stimulated radiation," Curr. Opin. Chem. Biol. **15**(6), 831–837 (2011).
2. X. Fan, I. M. White, S. I. Shopova, H. Zhu, J. D. Suter, and Y. Sun, "Sensitive optical biosensors for unlabeled targets: a review," Anal. Chim. Acta **620**(1-2), 8–26 (2008).
3. X. Fan and I. M. White, "Optofluidic microsystems for chemical and biological analysis," Nat. Photonics **5**(10), 591–597 (2011).
4. C. Ciminelli, C. M. Campanella, F. Dell'Olio, C. E. Campanella, and M. N. Armenise, "Label-free optical resonant sensors for biochemical applications," Prog. Quantum Electron. **37**(2), 51–107 (2013).
5. J. Yao, M. E. Stewart, J. Maria, T.-W. Lee, S. K. Gray, J. A. Rogers, and R. G. Nuzzo, "Seeing molecules by eye: surface plasmon resonance imaging at visible wavelengths with high spatial resolution and submonolayer sensitivity," Angew. Chem. Int. Ed. Engl. **47**(27), 5013–5017 (2008).
6. B. Johansson, F. Höök, D. Klenerman, and P. Jönsson, "Label-free measurements of the diffusivity of molecules in lipid membranes," ChemPhysChem **15**(3), 486–491 (2014).
7. J. Ortega Arroyo, J. Andrecka, K. M. Spillane, N. Billington, Y. Takagi, J. R. Sellers, and P. Kukura, "Label-free, all-optical detection, imaging, and tracking of a single protein," Nano Lett. **14**(4), 2065–2070 (2014).
8. S. Wang, X. Shan, U. Patel, X. Huang, J. Lu, J. Li, and N. Tao, "Label-free imaging, detection, and mass measurement of single viruses by surface plasmon resonance," Proc. Natl. Acad. Sci. U.S.A. **107**(37), 16028–16032 (2010).
9. E. A. Lidstone, V. Chaudhery, A. Kohl, V. Chan, T. Wolf-Jensen, L. B. Schook, R. Bashir, and B. T. Cunningham, "Label-free imaging of cell attachment with photonic crystal enhanced microscopy," Analyst (Lond.) **136**(18), 3608–3615 (2011).
10. W. Wang, Y. Yang, S. Wang, V. J. Nagaraj, Q. Liu, J. Wu, and N. Tao, "Label-free measuring and mapping of binding kinetics of membrane proteins in single living cells," Nat. Chem. **4**(10), 846–853 (2012).
11. C. A. Lopez, G. G. Daaboul, R. S. Vedula, E. Özkumur, D. A. Bergstein, T. W. Geisbert, H. E. Fawcett, B. B. Goldberg, J. H. Connor, and M. S. Unlü, "Label-free multiplexed virus detection using spectral reflectance imaging," Biosens. Bioelectron. **26**(8), 3432–3437 (2011).
12. N. Danz, A. Kick, F. Sonntag, S. Schmieder, B. Höfer, U. Klotzbach, and M. Mertig, "Surface plasmon resonance platform technology for multi-parameter analyses on polymer chips," Eng. Life Sci. **11**(6), 566–572 (2011).
13. A. W. Peterson, M. Halter, A. Tona, K. Bhadriraju, and A. L. Plant, "Surface plasmon resonance imaging of cells and surface-associated fibronectin," BMC Cell Biol. **10**(1), 16 (2009).

#233348 - $15.00 USD Received 28 Jan 2015; revised 20 Feb 2015; accepted 20 Feb 2015; published 2 Mar 2015

14. M. M. A. Jamil, M. C. T. Denyer, M. Youseffi, S. T. Britland, S. Liu, C. W. See, M. G. Somekh, and J. Zhang, "Imaging of the cell surface interface using objective coupled widefield surface plasmon microscopy," J. Struct. Biol. **164**(1), 75–80 (2008).
15. B. Huang, F. Yu, and R. N. Zare, "Surface plasmon resonance imaging using a high numerical aperture microscope objective," Anal. Chem. **79**(7), 2979–2983 (2007).
16. F. Pillet, C. Romera, E. Trévisiol, S. Bellon, M.-P. Teulade-Fichou, J.-M. François, G. Pratviel, and V. A. Leberre, "Surface plasmon resonance imaging (SPRi) as an alternative technique for rapid and quantitative screening of small molecules, useful in drug discovery," Sens. Actuators B Chem. **157**(1), 304–309 (2011).
17. Y. Gao, Z. Xin, B. Zeng, Q. Gan, X. Cheng, and F. J. Bartoli, "Plasmonic interferometric sensor arrays for high-performance label-free biomolecular detection," Lab Chip **13**(24), 4755–4764 (2013).
18. J. Cuiffi, R. Soong, S. Manolakos, S. Mohapatra, and D. Larson, "Nanohole array sensor technology : multiplexed label-free protein binding assays," Proc. IFMBE **32**, 572–575 (2010).
19. J.-C. Yang, J. Ji, J. M. Hogle, and D. N. Larson, "Metallic nanohole arrays on fluoropolymer substrates as small label-free real-time bioprobes," Nano Lett. **8**(9), 2718–2724 (2008).
20. K. Kim, J. Yajima, Y. Oh, W. Lee, S. Oowada, T. Nishizaka, and D. Kim, "Nanoscale localization sampling based on nanoantenna arrays for super-resolution imaging of fluorescent monomers on sliding microtubules," Small **8**(6), 892–900 (2012).
21. W. Chen, K. D. Long, M. Lu, V. Chaudhery, H. Yu, J. S. Choi, J. Polans, Y. Zhuo, B. A. C. Harley, and B. T. Cunningham, "Photonic crystal enhanced microscopy for imaging of live cell adhesion," Analyst (Lond.) **138**(20), 5886–5894 (2013).
22. Y. Zhuo, H. Hu, W. Chen, M. Lu, L. Tian, H. Yu, K. D. Long, E. Chow, W. P. King, S. Singamaneni, and B. T. Cunningham, "Single nanoparticle detection using photonic crystal enhanced microscopy," Analyst (Lond.) **139**(5), 1007–1015 (2014).
23. G. G. Daaboul, A. Yurt, X. Zhang, G. M. Hwang, B. B. Goldberg, and M. S. Ünlü, "High-throughput detection and sizing of individual low-index nanoparticles and viruses for pathogen identification," Nano Lett. **10**(11), 4727–4731 (2010).
24. C. Grivas and M. Pollnau, "Organic solid-state integrated amplifiers and lasers," Laser Photon. Rev. **6**(4), 419–462 (2012).
25. M. Lu, S. S. Choi, U. Irfan, and B. T. Cunningham, "Plastic distributed feedback laser biosensor," Appl. Phys. Lett. **93**(11), 111113 (2008).
26. C. Vannahme, M. C. Leung, F. Richter, C. L. C. Smith, P. G. Hermannsson, and A. Kristensen, "Nanoimprinted distributed feedback lasers comprising TiO_2 thin films: Design guidelines for high performance sensing," Laser Photon. Rev. **7**(6), 1036–1042 (2013).
27. E. Heydari, J. Buller, E. Wischerhoff, A. Laschewsky, S. Döring, and J. Stumpe, "Label-free biosensor based on an all-polymer DFB laser," Adv. Opt. Mater. **2**(2), 137–141 (2014).
28. T. Rabe, K. Gerlach, T. Riedl, H.-H. Johannes, W. Kowalsky, J. Niederhofer, W. Gries, J. Wang, T. Weimann, P. Hinze, F. Galbrecht, and U. Scherf, "Quasi-continuous-wave operation of an organic thin-film distributed feedback laser," Appl. Phys. Lett. **89**(8), 081115 (2006).
29. C. Vannahme, C. L. C. Smith, M. B. Christiansen, and A. Kristensen, "Emission wavelength of multilayer distributed feedback dye lasers," Appl. Phys. Lett. **101**(15), 151123 (2012).
30. M. B. Christiansen, T. Buß, C. L. C. Smith, S. R. Petersen, M. M. Jørgensen, and A. Kristensen, "Single mode dye-doped polymer photonic crystal lasers," J. Micromech. Microeng. **20**(11), 115025 (2010).
31. I. D. Block, P. C. Mathias, S. I. Jones, L. O. Vodkin, and B. T. Cunningham, "Optimizing the spatial resolution of photonic crystal label-free imaging," Appl. Opt. **48**(34), 6567–6574 (2009).
32. W. M. Haynes, ed., *CRC Handbook of Chemistry and Physics*, 93rd ed. (CRC, 2012).

1. Introduction

Dissolution of solid material in liquids, fluid flow, and mixing are important for processes in chemistry, food production, and medicine, especially for drug delivery. In addition, in the growing fields of microfluidics and lab on a chip, dissolution and flow dynamics are essential. Thus, there is a great interest in monitoring such processes. However, with standard imaging the presence of small molecules such as glucose or bovine serum albumin (BSA) and ions (e.g. Na^+, Cl^-, K^+, and Ca^{2+}) dissolved in liquids can often not be visualized as particle sizes are small and concentrations low. Labels, especially fluorescent labels, can be used for visualization of molecules when these have a much larger molecular weight than the labels. For small molecules however, labels affect diffusion and convection properties and labelling is not feasible for ions at all. On the other hand, microscopy techniques based on stimulated Raman scattering and stimulated emission allow label-free detection [1] but the imaging rate of these techniques is currently limited by the need for scanning.

Label-free surface refractive index detection based on optical signal transducers enables the detection of small molecules and ions with very low detection limits [2–4]. Recently, it has been shown that refractive index and refractive index changes can be imaged by spatially resolving optical resonances and resonance shifts [5–9]. This allows e.g. for studying

#233348 - $15.00 USD Received 28 Jan 2015; revised 20 Feb 2015; accepted 20 Feb 2015; published 2 Mar 2015

adhesion [9] and migration [10] of cells and for multiplexed biosensing [11,12]. Refractometric imaging has been demonstrated with optical signal transducers based on surface plasmon resonance [8,12–16], plasmonic hole arrays [17–20], passive photonic crystals [9,21,22], and interferometery [7,11,23].

For studying dissolution and fluid dynamics, low detection limits and high frame rates are required. For this purpose, dye-based distributed feedback (DFB) laser sensors are most suitable as optical signal transducers as they exhibit very low detection limits [24–27] and can be operated with very high repetition rates of up to 5 MHz [28]. As these lasers emit nanosecond pulses, integration times can be very short. In addition, DFB dye laser sensors feature low-cost materials and mass production replication technologies. With these sensors, changes imparted on the devices are detected by measuring shifts of the laser emission wavelength within the range of the evanescent field of the guided optical mode, corresponding to the first few hundred nanometers from the surface.

In this article, real-time dissolution monitoring of solid pieces of NaCl, sucrose, and BSA in water is presented utilizing DFB dye laser sensors in an optical imaging spectroscopy setup. It is demonstrated how these different materials show characteristic dissolution patterns. A high frame rate of 20 Hz is proven to enable the monitoring of fast flow of a sucrose solution jet into pure water.

2. DFB dye laser sensors and imaging spectroscopy setup

2nd order DFB laser devices were fabricated by spin-coating a Pyrromethene 597 doped Ormocomp thin film on glass, which was subsequently structured by UV nanoimprint and covered with a thin film of TiO_2, see Fig. 1(a). The thickness of the Ormocomp film was 400 nm and 25 nm for TiO_2, respectively. The size of the single grating structures for distributed feedback was 2 mm × 2 mm while the grating depth was approx. 100 nm. The grating period of Λ = 368 nm defines the emission wavelength of the lasers to approx. 563 nm with aqueous solution as a cladding. As the laser is a 2nd order DFB laser, feedback is provided by the grating in plane while the grating is also decoupling a part of the laser light orthogonally to the substrate plane. This decoupled light is used for detection. Further details of the fabrication process and the fundamentals of the DFB lasers are published elsewhere [26,29,30].

#233348 - $15.00 USD Received 28 Jan 2015; revised 20 Feb 2015; accepted 20 Feb 2015; published 2 Mar 2015

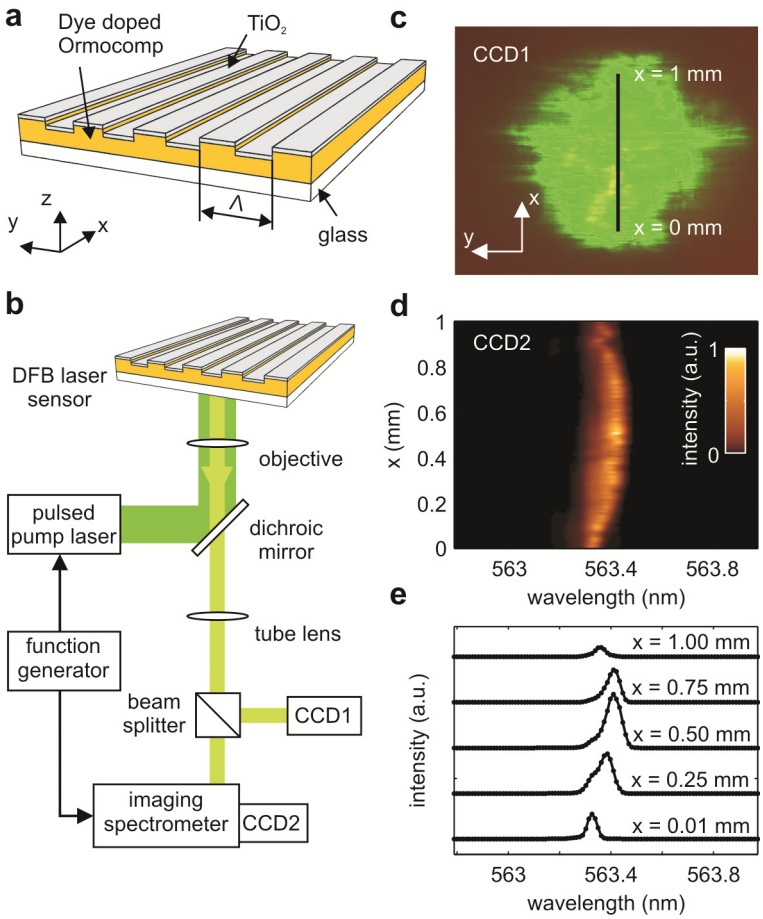

Fig. 1. Device and optical setup. (a) Schematic of DFB dye laser sensor with grating period Λ = 368 nm. (b) Schematic illustration of the optical setup. (c) Image of laser emission on the device surface. The black line indicates the position of the spectrometer entrance slit in the optical setup. (d) Typical image from CCD2 with narrow laser line in the center. Only a part of the image in wavelength direction is shown. (e) Spectra for five selected x-positions in (d).

The optical imaging spectroscopy setup is schematically illustrated in Fig. 1(b). It enables spatially resolving the laser emission wavelengths on a 1 mm long line. For excitation, a pump laser (CryLaS FDSS532-150) emitting 1 ns pulses at 532 nm is focused through a microscope objective onto the DFB laser. Reflected pump laser light is blocked by a dichroic mirror while the DFB laser emission is transmitted and used to project an image of the laser surface onto the control CCD array, CCD1. An image of the laser light on the DFB laser's surface with deionized (DI) water on top is shown in Fig. 1(c). In the optical setup, a duplicated image of the device surface is projected via a beam splitter onto the entrance slit of an imaging spectrometer with a 1800 g/mm grating giving a wavelength resolution of 12 pm/pixel on the CCD (Acton SP-2756 imaging spectrograph with PIXIS100B digital CCD camera, 100 × 1340 pixels, CCD2). Pump laser and CCD2 are triggered with the same signal from a function generator such that the laser pulse hits CCD2 during the integration time and not during read-out. Because of the triggering, the integration time could be reduced to 5 ms which significantly decreases noise compared to longer integration times. The laser is oriented such that the grating line direction in the image is parallel to the entrance slit. This gives a better spatial resolution than the orthogonal direction where the resolution is limited by the mode propagation [31]. The plot in Fig. 1(d) illustrates typical data obtained from CCD2. In Fig. 1(e), selected spectra for five x-positions are plotted showing the narrow

#233348 - $15.00 USD Received 28 Jan 2015; revised 20 Feb 2015; accepted 20 Feb 2015; published 2 Mar 2015

linewidth of the laser emission and nearly no background noise. E.g., the FWHM for the line at x = 0.5 mm is 0.07 nm. The CCD array records 100 spectra corresponding to the 100 pixels of one row in *x*-direction. The microscope setup gives 4 × magnification and as the spectrometer entrance slit is 4 mm long, the line scanned is 1 mm long with the width of one row corresponding to 10 µm. This defines the spatial resolution of the refractometric monitoring. In general, the spatial resolution depends on the resolution of the optical system and the resolution of the distributed feedback laser sensor. It can be expected that the light is not coupled in the scanning direction [31] and that the spatial resolution is thus the resolution of the imaging system. In this context, it is limited by the microscope optics and the number of pixels of the spectrometer CCD in *x*-direction. The spatial resolution could thus be enhanced by using a larger magnification and a CCD with more pixels in *x*-direction. Here, a 4 × magnification has been chosen to scan the comparably long distance of 1 mm. Concentration changes of the liquid on top of the laser result in well-known refractive index changes of the liquid for e.g. NaCl and sucrose [32]. A change of the refractive index causes the narrow laser line to shift with a sensitivity of approx. 90 nm/RIU. This can be detected with high resolution giving a detection limit of down to $8 \cdot 10^{-6}$ RIU, see [26] for a detailed discussion of the detection limit. In order to reach this detection limit, the center emission wavelength is calculated with a center-of-mass approach. Using all 100 rows of the CCD array, the center emission wavelength for 100 positions is obtained and wavelength shifts can be monitored in time and space. The maximum frame rate of the monitoring is limited to 12 Hz by the read-out time of the complete CCD2. The frame rate can be increased when only a part of the CCD array is read which is possible with the software of the PIXIS100B digital CCD.

3. Experiments

The fluidic structure used for the experiments in this work is illustrated in Fig. 2(a) with a photograph and as a schematic. It features fluidic wells which were fabricated by laser cutting of 1 mm thick PMMA slides. These slides were attached to the laser device with adhesive film. The structure exhibits a larger well of 4 mm diameter with the laser nanostructure in the center. A smaller well of 2 mm diameter is connected to the larger well by a 0.4 mm wide gap. This structure allows a controlled addition of solid material to the small well. Two smaller wells were present in the actual devices as it can be seen from the photograph but only one of them was used here.

Two types of experiments were performed: In the first type, the larger and a smaller well were both filled with water and a small piece of solid material was added to the smaller well. Thereupon, the dissolution of the material in water was monitored at the position of the laser grating. In the second experiment, only the large well was filled with water while the smaller well was empty. Due to its surface tension water is not flowing into the smaller well. Water with sucrose dissolved in it was added to the smaller well causing a fast stream of this sucrose solution into the large well which was monitored with the DFB laser sensor.

3.1 Dissolution monitoring

Figure 2 illustrates a typical result from the first type of experiment, the dissolution of different solid materials in water, where the dissolution of NaCl is shown in Fig. 2(b). The amount of solid material added was in the sub-mg range with particle diameters of less than 1 mm for all materials and experiments reported in the following. In Fig. 2(b), a surface plot of the wavelength shift as function of time and position illustrates how dissolved NaCl reached the *x*-positions closer to the small well first. The center wavelength was obtained from the spectra for each row of CCD2 by calculating the center of mass of the laser line. White symbols indicate the onset of the wavelength shift and the green line is a polynomial fit to these points. The same experiment was also performed with a larger amount of NaCl and even though the amount of NaCl was larger, a similar onset curve occurred while the absolute wavelength shift was stronger. Also sucrose and BSA were investigated. For comparison of the characteristic onset curves, they are plotted in Fig. 2(c) for the two amounts of NaCl,

#233348 - $15.00 USD Received 28 Jan 2015; revised 20 Feb 2015; accepted 20 Feb 2015; published 2 Mar 2015

sucrose, and BSA. For an easier comparison, the 4 onset curves in Fig. 2(c) have been shifted in time such that they begin at the same point in time. The different materials exhibit unique onset curves. This can be explained with different dissolution rates and diffusion coefficients of the compounds in water. The slight difference between the two onset curves for NaCl could be explained with the different amounts but also with how the NaCl was added and at which position in the smaller well it was dissolving.

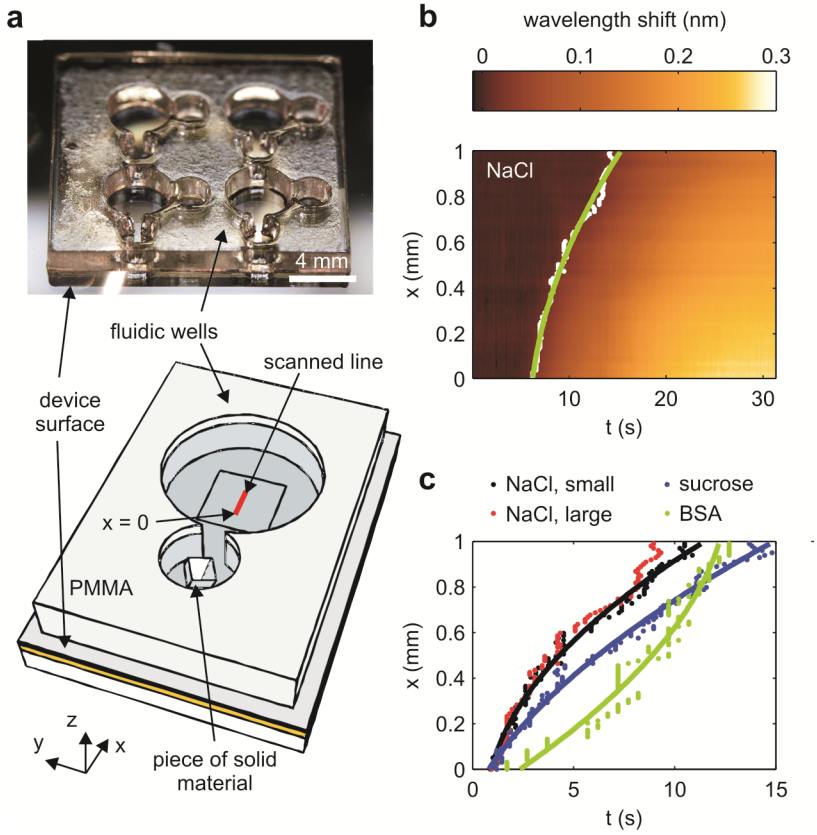

Fig. 2. Monitoring the dissolution of small pieces of solid materials in water with DFB dye laser sensors. (a) Schematic of fluidic well structure with laser area in the center and photograph of 4 of such well structures on the device. (b) Wavelength shift as function of time and position for adding a piece of NaCl to the small well. The white symbols indicate the onset of the wavelength shift and the green line is a fit to these data. Media 1 shows how the laser line shifts upon the presence of NaCl in the water, recorded with CCD2. (c) Comparison of onset lines for NaCl, sucrose, and BSA.

3.2 Fluid flow monitoring

The optical setup used here is capable of recording with a frame rate of up to 20 Hz limited by the read-out time of CCD2. To achieve a frame rate of 20 Hz the number of read pixels of CCD2 was reduced to 200 in the wavelength direction using the software *LightField* (Princeton Instruments) such that only the region where the laser line is present is analyzed. This allows studying faster refractive index changes than those that occur during dissolution of solid materials as shown so far. For investigation of fast fluid flow, the larger well of the fluidic structure shown in Fig. 2(a) was filled with water while the smaller well was kept empty. For illustration of the second type of experiment, a drop of water containing rhodamine 6G dye was added to the smaller well which caused a jet of this water flowing into the larger well. This was visualized in a fluorescence microscope setup, see Fig. 3(a). For this,

#233348 - $15.00 USD Received 28 Jan 2015; revised 20 Feb 2015; accepted 20 Feb 2015; published 2 Mar 2015

a video had been recorded with a high frame rate camera and the times given in Fig. 3(a) are corresponding to the respective frames of this video.

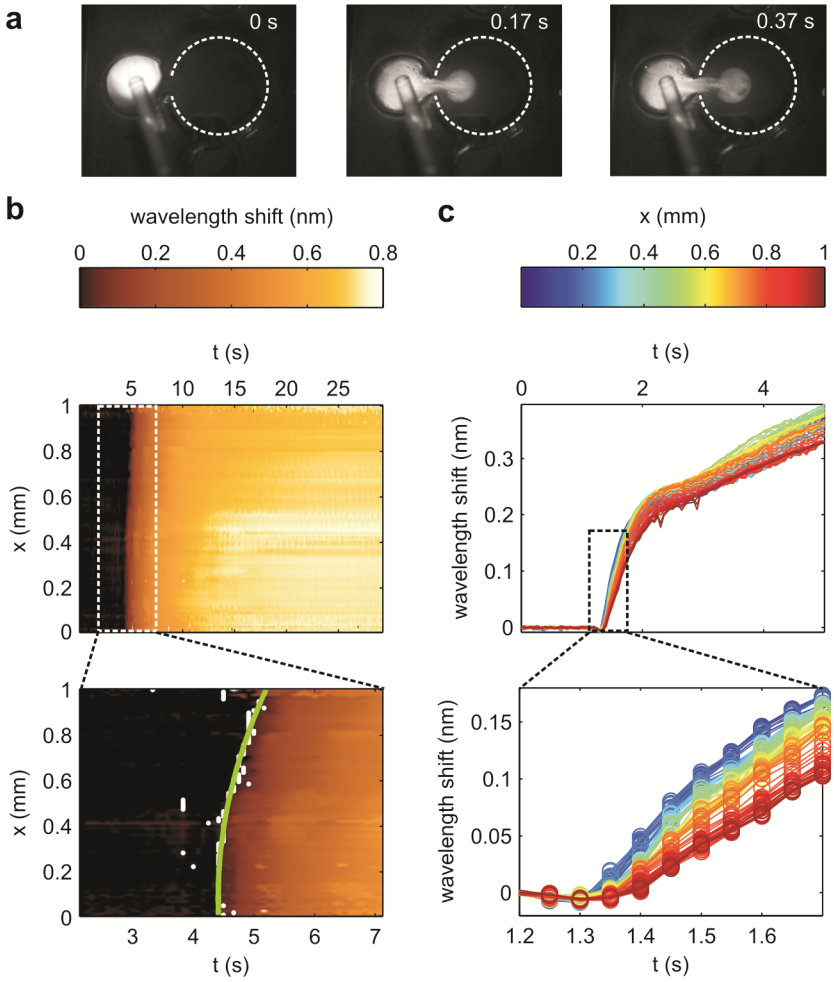

Fig. 3. Monitoring fast flow with DFB dye laser sensor. (a) A drop of water containing rhodamine 6G dye added to the empty smaller well (compare Fig. 2(a)) causing a jet stream into the larger well (dotted white line) filled with water. Media 2 shows this as a video. (b) Wavelength shift upon adding of sucrose water to the small well monitored with a frame rate of 12 Hz. (c) Wavelength shift upon addition of sucrose water to the small well monitored with a frame rate of 20 Hz.

However, if the added liquid is transparent such a process cannot easily be monitored with bright field or fluorescence microscopy. Here, it is presented how the same experiment with sucrose solution can be monitored with DFB laser sensors. It is illustrated in Figs. 3(b) and 3(c) how sucrose solution was added, causing a fast wavelength shift along the 1 mm long scanned line. For Fig. 3(b), a sucrose concentration in water of 0.13 g/ml was used and the process was recorded with a frame rate of 12 Hz. Here, the time is calculated from the frame rate given by the function generator where the time difference between adjacent frames is 1/12 s. The bigger well was filled with 20 µl of water and 6 µl of sucrose solution were added. It is evident from the two plots that the wavelength change was occurring much faster than in the experiments before. A line indicating the onset of the wavelength shift is shown again in Fig. 3(b), lower graph. When adding the liquid an irreproducible flow pattern occurs which is very sensitive to small changes on how the fluid is added. This becomes clear from

#233348 - $15.00 USD Received 28 Jan 2015; revised 20 Feb 2015; accepted 20 Feb 2015; published 2 Mar 2015

the data shown in Fig. 3(c) which corresponds to the same kind of experiment, this time monitored with a frame rate of 20 Hz. Here, the sucrose concentration in water was 0.1 g/ml. The lower inset in Fig. 3(c) illustrates the time resolution of the monitoring with symbols for each point in time.

4. Conclusion

In summary, highly sensitive refractometric imaging with DFB dye laser sensors has been demonstrated by monitoring the dissolution of small molecules and ions in water, and by monitoring the fast flow of a sucrose solution jet into pure water. The presented technique has substantial potential as it allows studying the dissolution of various kinds of materials and especially small molecules and ions in different optically transparent liquids and potentially also in solid matrices. The high frame rate of up to 20 Hz enables monitoring of fluid dynamics and the frame rate itself could be increased further by using a CCD array with faster read-out. In addition, the dye laser sensor provides both low detection limits and high spatial resolution. The presented method can readily be modified to operate on smaller or longer length scales and also potentially enhanced spatial resolution by using a microscope objective with different magnification.

Acknowledgments

The authors gratefully acknowledge fruitful discussion with Prof. Rodolphe Marie and thank him for providing BSA. C.V. acknowledges support from the Danish Research Council for Technology and Production Sciences (Grant no. 12-126676). The authors gratefully acknowledge funding from the European Commission under the Seventh Framework Programme (FP7/2007–2013) under grant agreements number 278204 (Cellomatic) and from the Strategic Research Center PolyNano (10-092322).

#233348 - $15.00 USD Received 28 Jan 2015; revised 20 Feb 2015; accepted 20 Feb 2015; published 2 Mar 2015